HHS Public Access

Author manuscript

Inf Process Med Imaging. Author manuscript; available in PMC 2019 November 22.

Published in final edited form as:

Inf Process Med Imaging. 2019 ; 11492: 384–393. doi:10.1007/978-3-030-20351-1_29.

A longitudinal model for tau aggregation in Alzheimer's disease based on structural connectivity

Fan Yang[1,2], **Samadrita Roy Chowdhury**[1,2], **Heidi I. L. Jacobs**[2], **Keith A. Johnson**[2], and **Joyita Dutta**[1,2]

[1]Department of Electrical and Computer Engineering, University of Massachusetts Lowell, Lowell, MA, USA

[2]Massachusetts General Hospital & Harvard Medical School, Boston, MA, USA
dutta.joyita@mgh.harvard.edu

Abstract

Tau tangles are a pathological hallmark of Alzheimer?s disease (AD) with strong correlations existing between tau aggregation and cognitive decline. Studies in mouse models have shown that the characteristic patterns of tau spatial spread associated with AD progression are determined by neural connectivity rather than physical proximity between different brain regions. We present here a network diffusion model for tau aggregation based on longitudinal tau measures from positron emission tomography (PET) and structural connectivity graphs from diffusion tensor imaging (DTI). White matter fiber bundles reconstructed via tractography from the DTI data were used to compute normalized graph Laplacians which served as graph diffusion kernels for tau spread. By linearizing this model and using sparse source localization, we were able to identify distinct patterns of propagative and generative buildup of tau at a population level. A gradient descent approach was used to solve the sparsity-constrained optimization problem. Model fitting was performed on subjects from the Harvard Aging Brain Study cohort. The fitted model parameters include a scalar factor controlling the network-based tau spread and a network-independent seed vector representing seeding in different regions-of-interest. This parametric model was validated on an independent group of subjects from the same cohort. We were able to predict with reasonably high accuracy the tau buildup at a future time-point. The network diffusion model, therefore, successfully identifies two distinct mechanisms for tau buildup in the aging brain and offers a macroscopic perspective on tau spread.

Keywords

Alzheimer's disease; network diffusion; tau; structural connectivity; PET; DTI

1 Introduction

Alzheimer's disease (AD) is a progressive neurodegenerative disorder which is the leading cause of dementia in the elderly. Extracellular amyloid-β (Aβ) plaques and intracellular tau neurofibrillary tangles, the two hallmark pathologies of this disease, are believed to play a key mechanistic role in AD [8]. Studies show that misfolded tau pathology in the medial temporal lobe is an important biomarker for neurodegeneration in preclinical AD [3]. Unlike

Aβ, tau exhibits an anatomically stereotypical propagation pattern in the brain. A growing body of evidence indicates that tau spreads through the brain from neurons to nearby neurons in a prion-like fashion [5,11–14]. Studies in mouse models have shown that the characteristic patterns of tau spatial spread associated with AD progression are determined by neural connectivity rather than physical proximity between different brain regions [1]. Comprehension of neurodegenerative pathogenesis requires the understanding of proliferation and accumulation mechanisms of tau [10]. Network diffusion models [7,17,18] have had reasonable success predicting dementia patterns and as well as modeling the relationship between structural and functional connectivity in the human brain. In this paper, we present a network diffusion model for tau propagation that seeks to characterize – at a macroscopic level – its relationship with the axonal pathway distributions captured by the brain's structural connectivity network.

In recent years, a number of novel positron emission tomography (PET) radiotracers have enabled *in vivo* visualization of tau burden. Recent studies report that ^{18}F-flortaucipir PET imaging of tau [20] allows *in vivo* Braak staging based on tracer uptake measures and that the spatial distribution patterns of the tracer mirror clinical and neuroanatomical variability in AD [9,15,19]. Here we use longitudinal ^{18}F-flortaucipir tau PET data collected at two time-points for obtaining regional tau measures. White matter fiber bundles generated via diffusion tensor imaging (DTI) are used to compute the structural connectivity network graphs for each subject.

In section 2, we present the derivation and implementation of the network diffusion model. The data processing and analysis details are provided in section 3, while our main findings are reported in section 4. In section 5, we summarize this work, discuss its strengths and limitations, and present our envisioned future directions.

2 Theory

2.1 Network Diffusion Model

We model the accumulation of tau as a diffusion process on a brain network graph defined as $\mathcal{G} = (\mathcal{V}, \mathcal{E})$ where the ith node, $v_i \in \mathcal{V}$, represents the ith gray matter parcellation or region-of-interest (ROI), $|\mathcal{V}| = N$ is the number of ROIs, and $\epsilon_{ij} \in \mathcal{E}$ represents fiber connectivity between node v_i and node V_j. The regional tau burden is a time-varying signal defined on the graph G and can be represented as a vector $x(t) = \{x(v_i, t), v_i \in \mathcal{V}\}, x(t) \in \mathbb{R}^N$. **x**(t) is the solution to a first order partial differential equation, usually referred to as the *network diffusion equation*:

$$\frac{\partial x(t)}{\partial t} = -\beta L x(t), \quad (1)$$

where $L \in \mathbb{R}^{N \times N}$ is the static graph Laplacian matrix based on DTI, which captures the structural connectivity of an individual subject's brain. Solutions to (1) are of the form:

$$x(t) = e^{-\beta L\left(t - t_0\right)} x\left(t_0\right), \quad (2)$$

where $\mathbf{x}(t_0)$ is the initial tau burden at time t_0. To model proteopathic tau seeding [6] in addition to network-dependent spread, we add a source term $\mathbf{s}(t)$ to (1) as follows:

$$\frac{\partial x(t)}{\partial t} = -\beta L x(t) + s(t). \quad (3)$$

For $s(t) = \alpha\delta\left(t - t_0^+\right)$, an impulsive source at $t = t_0^+$, the solution to this equation

$$x(t) = e^{-\beta L\left(t - t_0\right)} x_{\mathbf{0}} + e^{-\beta L\left(t - t_0^+\right)} \alpha u\left(t - t_0^+\right), \quad (4)$$

where $u\left(t - t_0^+\right)$ is the unit step function at t_0^+. In subsequent analyses, we replace t_0^+ with t_0 in the second term.

2.2 Longitudinal Two Time-Point Model

For longitudinal two time-point tau PET datasets, t_0 represents the time-point at which a baseline tau PET scan is performed and t represents a second time-point at which either a follow-up tau PET scan is performed or at which the tau burden is to be predicted using the network diffusion model. For simplicity, we denote the tau buildup at t_0 and t by $\boldsymbol{x}_0$ and $\boldsymbol{x}_t$ respectively and the time gap as $\Delta t = t - t_0$. For preclinical AD, tau accumulation occurs at a slow rate. Using this rationale, we linearize (4) via the relationship:

$$e^{-\beta L\left(t - t_0\right)} \simeq I - \beta L\left(t - t_0\right). \quad (5)$$

Accordingly, the solution can be approximated as:

$$x_t = [I - \beta L \Delta t]\left(x_0 + \alpha\right). \quad (6)$$

For ease of notation, we denote:

$$H(\beta) = I - \beta L \Delta t. \quad (7)$$

We can estimate the parameters $\boldsymbol{\alpha}$ and $\boldsymbol{\beta}$ by minimizing the data fidelity cost function:

$$\min_{\beta,\alpha}\frac{1}{2}\left\|H(\beta)\left(x_0+\alpha\right)-x_t\right\|_2^2. \quad (8)$$

The unknowns in this model are $\boldsymbol{\alpha}$ and $\boldsymbol{\beta}$. For group-level prediction, we extend (8), which is an individual model, to a jointly fitted model for the entire cohort where, $k = 1, 2,\ldots M$, M being the number of subjects. We modify (7) to incorporate the index k as follows:

$$H^{(k)}(\beta) = I - \beta L^{(k)}\Delta t^{(k)}. \quad (9)$$

The new group-level data fidelity cost function is as follows:

$$\Phi_{DF}(\alpha,\beta) = \sum_k \frac{1}{2}\left\|H^{(k)}(\beta)\left(x_0^{(k)}+\alpha\right)-x_t^{(k)}\right\|_2^2. \quad (10)$$

To ensure a spatially sparse distribution of tau seeds, we introduce an L^1 penalty on $\boldsymbol{\alpha}$. To ensure small values of $\boldsymbol{\beta}$, which is the basis of linearization, we introduce an L^2 penalty on $\boldsymbol{\beta}$. The penalty terms are grouped together as a combined regularization function given by:

$$\Phi_R(\alpha,\beta) = \lambda_1|\alpha| + \frac{1}{2}\lambda_2\beta^2, \quad (11)$$

where λ_1 and λ_2 are regularization parameters.

2.3 Implementation

We use an alternating gradient descent strategy to solve the associated constrained optimization problem:

$$(\hat{\alpha},\hat{\beta}) = \arg\min_{\alpha\geq\mathbf{0},\beta\geq 0}\Phi(\alpha,\beta), \quad (12)$$

$$\Phi(\alpha,\beta) = \Phi_{DF}(\alpha,\beta) + \Phi_R(\alpha,\beta). \quad (13)$$

The partial derivatives with respect to $\boldsymbol{\beta}$ are computed as follows:

$$\frac{\partial\Phi_{DF}}{\partial\beta} = \sum_k\left[-\Delta t^{(k)}L^{(k)}\left(x_0^{(k)}+\alpha\right)\right]^T\left[H^{(k)}(\beta)\left(x_0^{(k)}+\alpha\right)-x_t^{(k)}\right], \quad (14)$$

$$\frac{\partial \Phi_R}{\partial \beta} = \lambda_2 \beta . \quad (15)$$

The partial gradients with respect to $\boldsymbol{\alpha}$ are computed as follows:

$$\nabla_\alpha \Phi_{DF} = \sum_k \left[H^{(k)}\right]^T \left[H^{(k)}(\beta)\left(x_0^{(k)} + \alpha\right) - x_t^{(k)}\right], \quad (16)$$

$$\nabla_\alpha \Phi_R = \lambda_1 \mathbf{1}, \quad (17)$$

where **1** represents a vector with all entries equal to the number 1. In deriving (17), we rely on the fact that our constrained optimization algorithm restricts the solution for $\boldsymbol{\alpha}$ to the non-negative orthant where the L^1 norm is differentiable.

3 Experiments

3.1 Data Description

All experiments relied on data from the Harvard Aging Brain Study (HABS) [4], which is an ongoing longitudinal study aimed at revealing the differences between normal aging and preclinical AD. Datasets available from this study include longitudinal data of neuropsychological scores as well as multimodality neuroimaging data.

3.2 Subject Information

We applied the model to 62 subjects (75.85 ±6.18 years, 37 females) from HABS with Tl-weighted high-resolution anatomical MR images, diffusion MR images, and two time-point ^{18}F-flortaucipir PET scans for tau.

3.3 Data Acquisition and Processing

The overall data preprocessing workflow is depicted in Fig. 1. All MR imaging was performed on a Siemens Tim Trio 3T MR scanner with a 12-channel phased-array head coil. High-resolution, T1-weighted MR images were obtained using an MPRAGE pulse sequence.

DTI Processing—Diffusion MRI data preprocessing comprised correction of subject motion, eddy current distortion correction, and tensor model estimation. The first two steps were performed using FSL [2] while the last step was processed in MedINRIA [21]. We also enabled the embedded feature of automatic brain extraction during tensor model estimation. Diffusion tensor maps of fractional anisotropy (FA), mean diffusivity, axial diffusivity, and radial diffusivity were computed. After DTI data preprocessing, deterministic tractography was performed using MedINRIA. Tractography comprises seeding, propagation, and termination of streamlines indicative of fiber pathways. The seeding and termination of these

pathways is determined by the starting and stopping FA threshold values, which were set at 0.07 and 0.1 respectively in accordance with literature-suggested numbers for the adult brain. The minimum length for a streamline to be considered a valid representation of a fiber pathway was set to 10 mm.

To adjust for linear shifts in head position and scale within the same subject, each T1-weighted scan was registered to the corresponding diffusion MR scans using FSL with 9-parameter registration based on a mutual information cost function. We retained only the tracts starting and ending at the 112 FreeSurfer-defined cortical and subcortical ROIs. The reconstructed streamlines or tracts were counted for each pair of ROIs leading to pairwise connection strengths used to construct a 112 × 112 adjacency matrix.

PET Acquisition and Processing—PET images were acquired on a Siemens (Knoxville, TN) ECAT HR+ scanner (3D mode, 63 image planes, 15.2-cm axial field of view, 5.6-mm transaxial resolution, and 2.4-mm slice interval). ^{18}F-flortaucipir scans were performed 80 – 100 min after a 9.0 – 11.0 mCi bolus injection in four 5-minute frames.

Each attenuation-corrected PET image frame was verified for adequacy of counts and absence of head motion during imaging. For anatomical reference, the ^{18}F-flortaucipir PET image from each subject was rigidly co-registered with the corresponding T1-weighted MR image using SPM8 [16]. FreeSurfer ROIs were mapped into the PET native space.We calculate the standardized uptake value ratio (SUVR) for each of the 112 ROIs using FreeSurfer's cerebellar gray ROI mean as the reference.

4 Results

4.1 Parameter Estimation

The model parameters α and β were computed from two time-point data for the 62-subject cohort described in section 3.2. Fig. 2 shows the differential aggregation of tau across the two time-points averaged over the cohort and split into propagative and generative components. Tau aggregation in disparate regions of the brain is differently impacted by the diffusive spread vs. generative buildup. Consistent with our understanding of early AD, some of the strongest seeding effects were observed in several medial temporal areas such as the inferior temporal lobe, fusiform gyrus, entorhinal cortex, and the parahippocampal gyrus. Several limbic and subcortical regions also exhibited prominent roles in tau seeding.

4.2 Model Validation

Model parameters estimated for the 62-subject-group were validated using an independent group of 10 subjects. This validation dataset contained ^{18}F-flortaucipir PET scans at three distinct time-points (t_1, t_2, t_3). α and β computed from the 62-subject dataset were used to predict tau at t_2 from tau at t_1 and tau at t_3 from tau at t_2 for the 10-subject dataset. Fig. 3 shows predicted vs. observed scatter plots for time-point combinations (t_1, t_2) and (t_2, t_3). Table 1 shows goodness-of-fit measures for the predicted vs. observed data, including the sum of squares due to error (SSE), R^2, adjusted R^2, and root-mean-square error (RMSE). Our results indicate high prediction accuracy for (t_1, t_2) and diminished accuracy for (t_2, t_3).

5 Conclusion

We presented here a macroscopic model of tau spread and seeding based on structural networks derived from DTI and longitudinal tau measures based on ^{18}F-flortaucipir PET. The model relies on a linearized solution to the network diffusion equation and incorporates a spatially sparse source term capturing network-independent seeding. The model parameters were computed using data from 62 HABS subjects with diffusion MR data and two time-point ^{18}F-flortaucipir PET data. The fitted model parameters were validated on an independent group of 10 subjects with longitudinal ^{18}F-flortaucipir PET available at three time-points. The parametric model identified strong network-independent seeding in several anatomical areas believed to play prominent roles in preclinical AD.

One key limitation of the existing implementation is that it is based on a linear approximation motivated by the availability of only two temporal samples in the longitudinal tau PET study. Since the model parameters were estimated for an early cross-section of the preclinical AD population, the model's accuracy is expected to diminish for later disease stages. The model exhibited higher accuracy when applied to data from the first two time-points of the validation dataset. As expected, the accuracy was lower for data from the second and third time-points. It is understandable that, for these cases, the approximate linear model exhibits a greater divergence relative to the original exponential model.

We have demonstrated the effectiveness of a network diffusion approach to model and predict tau aggregation based on structural connectivity. Our model identified distinct patterns of network-based propagative and network-independent generative buildup of tau in an elderly cohort. Our future work would involve extending this implementation to fit a piecewise linear model to three time-point datasets as they gradually become available in greater numbers for the HABS cohort.

Acknowledgments

Supported by the National Institute on Aging grant K01AG050711

References

1. Ahmed Z, Cooper J, Murray TK, Garn K, McNaughton E, Clarke H, Parhizkar S, Ward MA, Cavallini A, Jackson S, Bose S, Clavaguera F, Tolnay M, Lavenir I, Goedert M, Hutton ML, O'Neill MJ: A novel in vivo model of tau propagation with rapid and progressive neurofibrillary tangle pathology: the pattern of spread is determined by connectivity, not proximity. Acta Neuropathol. 127(5), 667–683 (5 2014) [PubMed: 24531916]
2. Andersson JLR, Sotiropoulos SN: An integrated approach to correction for off-resonance effects and subject movement in diffusion MR imaging. Neuroimage 125, 1063–1078 (2016) [PubMed: 26481672]
3. Arriagada PV, Growdon JH, Hedley-Whyte ET, Hyman BT: Neurofibrillary tangles but not senile plaques parallel duration and severity of Alzheimer's disease. Neurology 42(3 Pt 1), 631–639 (3 1992) [PubMed: 1549228]
4. Dagley A, LaPoint M, Huijbers W, Hedden T, McLaren DG, Chatwal JP, Papp KV, Amariglio RE, Blacker D, Rentz DM, Johnson KA, Sperling RA, Schultz AP: Harvard Aging Brain Study: Dataset and accessibility. Neuroimage 144(Pt B), 255–258 (1 2017) [PubMed: 25843019]
5. Frost B, Diamond MI: Prion-like mechanisms in neurodegenerative diseases. Nat. Rev. Neurosci 11(3), 155–159 (3 2010) [PubMed: 20029438]

6. Holmes BB, Furman JL, Mahan TE, Yamasaki TR, Mirbaha H, Eades WC, Belaygorod L, Cairns NJ, Holtzman DM, Diamond MI: Proteopathic tau seeding predicts tauopathy in vivo. Proc. Natl. Acad. Sci. U.S.A 111(41), E4376–4385 (10 2014) [PubMed: 25261551]
7. Hu C, Hua X, Ying J, Thompson PM, Fakhri GE, Li Q: Localizing Sources of Brain Disease Progression with Network Diffusion Model. IEEE J. Sel. Top. Signal Process 10(7), 1214–1225 (10 2016) [PubMed: 28503250]
8. Hyman BT, Phelps CH, Beach TG, Bigio EH, Cairns NJ, Carrillo MC, Dickson DW, Duyckaerts C, Frosch MP, Masliah E, Mirra SS, Nelson PT, Schneider JA, Thal DR, Thies B, Trojanowski JQ, Vinters HV, Montine TJ: National Institute on Aging-Alzheimer's Association guidelines for the neuropathologic assessment of Alzheimer's disease. Alzheimers Dement. 8(1), 1–13 (1 2012) [PubMed: 22265587]
9. Johnson KA, Schultz A, Betensky RA, Becker JA, Sepulcre J, Rentz D, Mormino E, Chhatwal J, Amariglio R, Papp K, Marshall G, Albers M, Mauro S, Pepin L, Alverio J, Judge K, Philiossaint M, Shoup T, Yokell D, Dickerson B, Gomez-Isla T, Hyman B, Vasdev N, Sperling R: Tau positron emission tomographic imaging in aging and early Alzheimer disease. Ann. Neurol 79(1), 110–119 (1 2016) [PubMed: 26505746]
10. Kaufman SK, Del Tredici K, Thomas TL, Braak H, Diamond MI: Tau seeding activity begins in the transentorhinal/entorhinal regions and anticipates phospho-tau pathology in Alzheimer's disease and PART. Acta Neuropathol. 136(1), 57–67 (7 2018) [PubMed: 29752551]
11. Lace G, Savva GM, Forster G, de Silva R, Brayne C, Matthews FE, Barclay JJ, Dakin L, Ince PG, Wharton SB: Hippocampal tau pathology is related to neuroanatomical connections: an ageing population-based study. Brain 132(Pt 5), 1324–1334 (5 2009) [PubMed: 19321462]
12. Lee SJ, Desplats P, Sigurdson C, Tsigelny I, Masliah E: Cell-to-cell transmission of non-prion protein aggregates. Nat. Rev. Neurol 6(12), 702–706 (12 2010) [PubMed: 21045796]
13. Nussbaum JM, Schilling S, Cynis H, Silva A, Swanson E, Wangsanut T, Tayler K, Wiltgen B, Hatami A, Ronicke R, Reymann K, Hutter-Paier B, Alexandru A, Jagla W, Graubner S, Glabe CG, Demuth HU, Bloom GS: Prion-like behaviour and tau-dependent cytotoxicity of pyroglutamylated amyloid-β. Nature 485(7400), 651–655 (5 2012) [PubMed: 22660329]
14. Nussbaum JM, Seward ME, Bloom GS: Alzheimer disease: a tale of two prions. Prion 7(1), 14–19 (2013) [PubMed: 22965142]
15. Ossenkoppele R, Schonhaut DR, Scholl M, Lockhart SN, Ayakta N, Baker SL, O'Neil JP, Janabi M, Lazaris A, Cantwell A, Vogel J, Santos M, Miller ZA, Bettcher BM, Vossel KA, Kramer JH, Gorno-Tempini ML, Miller BL, Jagust WJ, Rabinovici GD: Tau PET patterns mirror clinical and neuroanatomical variability in Alzheimer's disease. Brain 139(Pt 5), 15511567 (5 2016) [PubMed: 26962052]
16. Penny WD, Friston KJ, Ashburner JT, Kiebel SJ, Nichols TE: Statistical parametric mapping: the analysis of functional brain images. Elsevier (2011)
17. Raj A, Kuceyeski A, Weiner M: A network diffusion model of disease progression in dementia. Neuron 73(6), 1204–1215 (3 2012) [PubMed: 22445347]
18. Raj A, LoCastro E, Kuceyeski A, Tosun D, Relkin N, Weiner M: Network diffusion model of progression predicts longitudinal patterns of atrophy and Metabolism in Alzheimer's disease. Cell Rep. (1 2015)
19. Schwarz AJ, Yu P, Miller BB, Shcherbinin S, Dickson J, Navitsky M, Joshi AD, Devous MD, Mintun MS: Regional profiles of the candidate tau PET ligand 18F-AV-1451 recapitulate key features of Braak histopathological stages. Brain 139(5), 1539–1550 (5 2016) [PubMed: 26936940]
20. Shoup TM, Yokell DL, Rice PA, Jackson RN, Livni E, Johnson KA, Brady TJ, Vasdev N: A concise radiosynthesis of the tau radiopharmaceutical, [(18) F]T807. J. Labelled Comp. Radiopharm 56(14), 736–740 (12 2013) [PubMed: 24339014]
21. Toussaint N, Souplet JC, Fillard P: MedlNRIA: Medical image navigation and research tool by INRIA. Med. Image Comput. Comput. Assist. Interv 7 (2007)

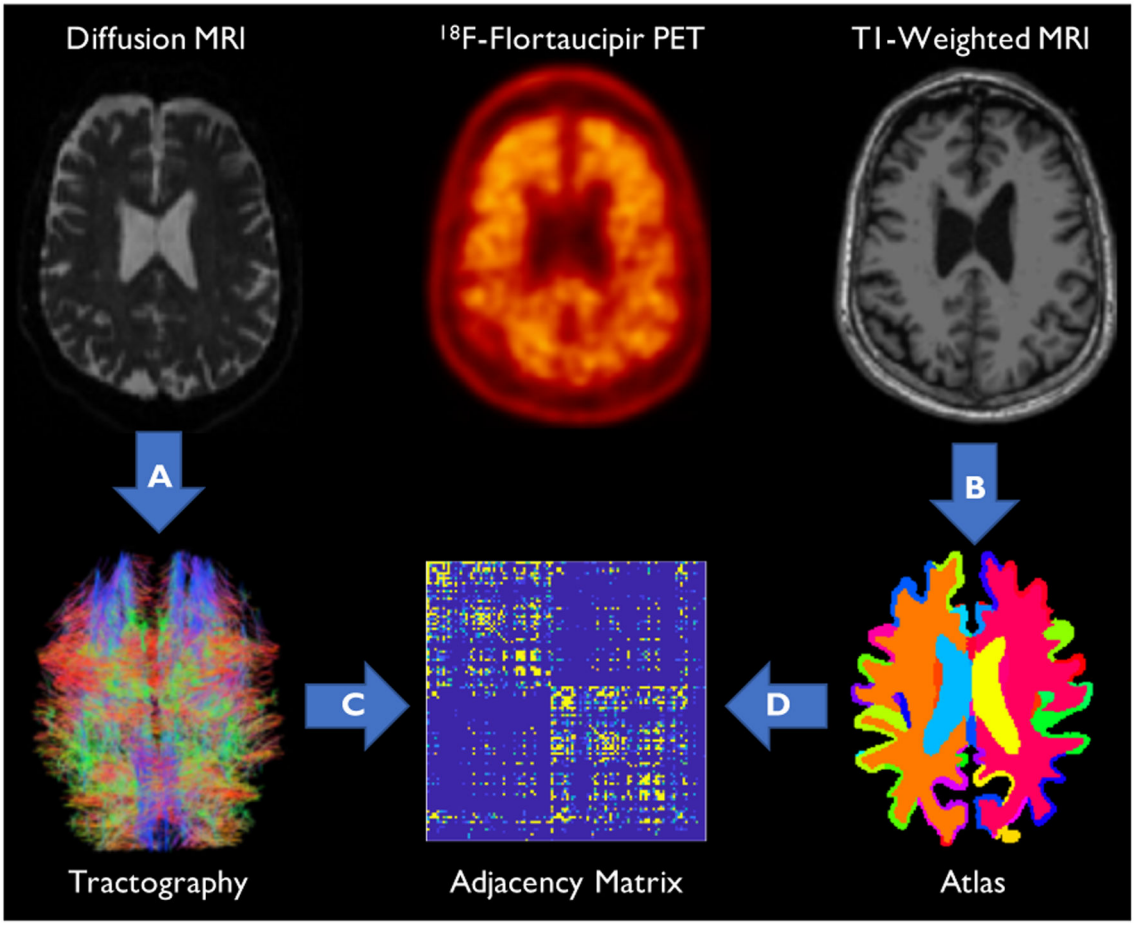

Fig. 1.

Sample ^{18}F-flortaucipir PET, diffusion MR, and Tl-weighted MR images, the FreeSurfer atlas, and a sample weighted adjacency matrix. White matter fiber tracts were reconstructed from the diffusion MR images via tractography (step A) using the software MedlNRIA. The T1-weighted anatomical reference images were segmented by means of deformable registration to match the FreeSurfer atlas (step B). Fiber counting was performed on the segmented diffusion image volumes to derive pairwise inter-region connection strengths thereby yielding an adjacency matrix (steps C and D). The mean ^{18}F-flortaucipir specific binding was computed for the FreeSurfer ROIs.

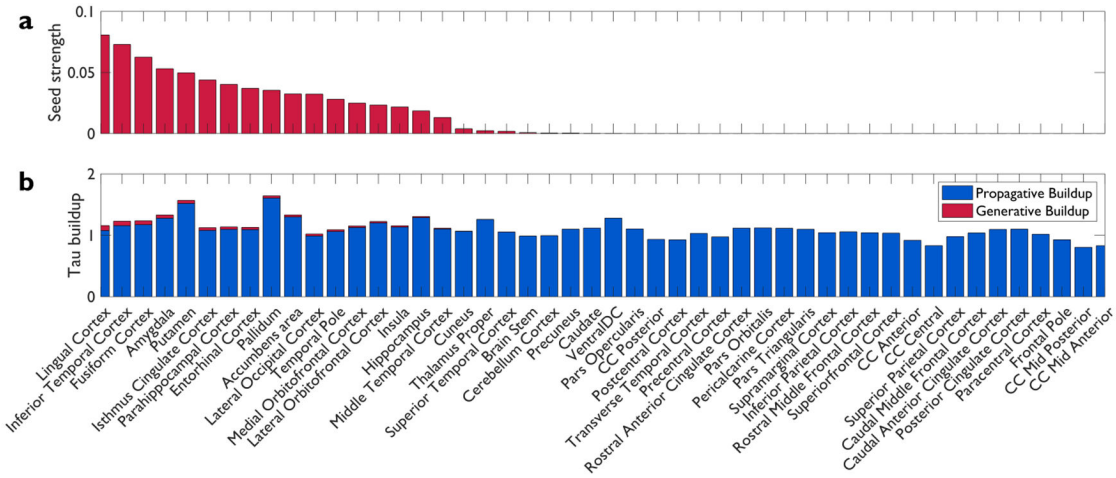

Fig. 2.

Tau seeding and spread at different ROIs. (a) Spatially sparse sources (localized seeds) identified by the network diffusion model sorted in descending order of strength. (b) The corresponding relative extents of tau buildup in different anatomical ROIs via spread alone (propagative buildup) and seeding-induced spread (generative buildup).

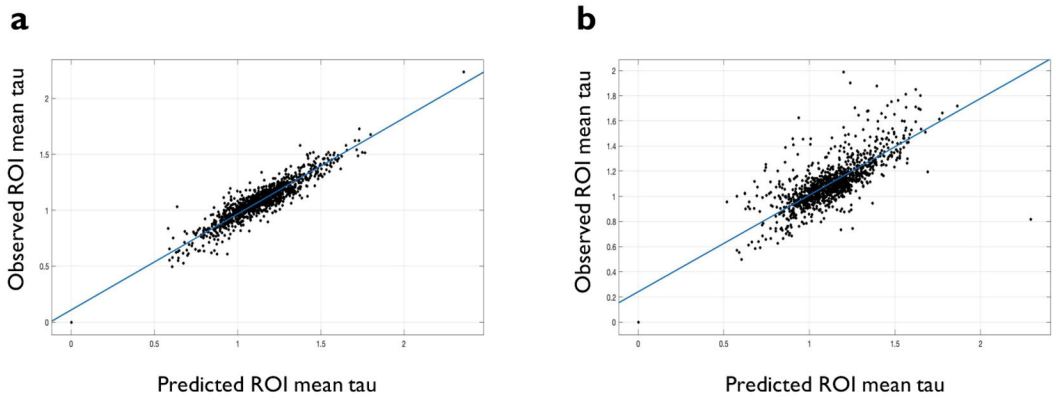

Fig. 3.

Scatter plots showing predicted vs. observed ROI mean tau values. (a) Tau at time-point t_2 predicted from tau at time-point t_1. (b) Tau at time-point t_3 predicted from tau at time-point t_2. Linear regression lines are shown in blue.

Table 1.

Model validation: Goodness-of-fit between predicted and observed tau

Time-points	SSE	R^2	Adjusted R^2	RMSE
(t_1, t_2)	5.449	0.8803	0.8802	0.0698
(t_2, t_3)	19.24	0.6207	0.6204	0.1312